JOURNAL OF MATERIALS SCIENCE, 33 (1998) 2499–2507

Chemical stability of MgO/CaO/Cr_2O_3–Al_2O_3–B_2O_3–phosphate glasses in solid oxide fuel cell environment

P. H. LARSEN
Materials Research Department, Risø National Laboratory, DK-4000 Roskilde, Denmark
P. F. JAMES
Centre for Glass Research, Department of Engineering Materials, University of Sheffield, Sir Robert Hadfield Building, Mappin St., Sheffield S1 3JD, UK
E-mail: p.f.james@sheffield.ac.uk

The thermal properties, glass forming tendency and glass stability in solid oxide fuel cell (SOFC) relevant atmospheres have been determined for four different refractory MgO/CaO/Cr_2O_3–Al_2O_3–B_2O_3 phosphate based glasses. Also, the bonding ability and interaction as a function of temperature between the glasses and $La_{0.8}Ca_{0.22}CrO_3$ interconnect material have been studied. The microstructural characterization and elemental analysis of reaction couples reveal that the bonding ability and interface interaction is closely related to the CaO content and the relative glass forming tendency. The reactions at 1000 °C between the glass and the solid interconnect material for the high CaO or MgO containing compositions occur by a liquid phase or a vapour phase mechanism, respectively. The reaction at 1200 °C in both cases occurs by a liquid phase mechanism. © *1998 Chapman & Hall*

1. Introduction

A solid oxide fuel cell (SOFC) is an electrochemical cell that directly converts the chemical energy of a fuel gas to electricity. To obtain sufficiently high voltages the cells are stacked in series as illustrated in Fig. 1, showing the flat plate planar cross flow design and the type of materials used in the Danish SOFC Programme [1]. To prevent the fuel gas and air from mixing during operation it is necessary to seal the electrodes: the cathode is to be sealed on the fuel inlet and outlet side and the anode is to be sealed on the air inlet and outlet side. Any leakage of fuel into the air (or air into the fuel) will lead to direct combustion and may cause local overheating (hot spots).

The purpose of sealing is thus to separate strongly reducing wet gasses (H_2, CO, CH_4) from air at the SOFC operating temperature. The sealing material will therefore be in intimate contact with stack components during operation (850–1000 °C) in an oxygen partial pressure in the range from 2×10^4 to 1×10^{-13} Pa (1000 °C). This results in a number of requirements that the sealing material must meet. The sealing material has to have a high chemical stability in air and in fuel gas over the entire temperature range 25–1000 °C, and limited chemical reactivity towards the other stack component materials is obviously of great importance. However, wetting capability against electrolyte, interconnect and manifold is also needed to ensure a tight seal in the contact between the seal and the components in question. A low vapour pressure in the relevant gases and in the entire temperature range is required to minimize loss by vapourization. Furthermore, the sealing material should have a suitable viscosity at the operating temperature, i.e. deformable but able to withstand a slight overpressure and a thermal expansion coefficient (TEC) that matches that of the other stack components.

It is generally agreed among SOFC developers that one of the main challenges encountered when building flat plate stacks is to obtain long term stable operational seals [2]. Due to the high degree of commercial interest, the issue of SOFC sealing is rarely discussed in the open literature. However, a few studies have been reported and silica based materials are usually considered as potential sealing materials for SOFC [3–8]. In the present study, four refractory phosphate based compositions have been studied. A Mg–Al–B–phosphate glass was chosen as the base composition. The choice was based on preliminary studies that revealed a relatively high refractoriness of this system. The objective of the present work was to explore and compare the effect of substituting MgO with CaO and addition of Cr_2O_3 on some of the SOFC relevant properties. CaO and Cr_2O_3 were chosen because of their presence in the interconnector material ($La_{0.8}Ca_{0.22}CrO_3$).

The investigation of the glasses is divided into four areas: a) characterization of the thermal properties by differential thermal analysis (DTA) and dilatometry, b) characterization of the glass forming tendency,

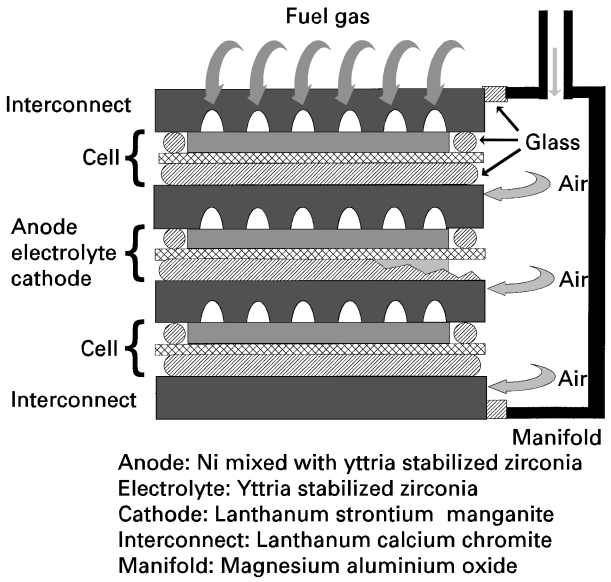

Figure 1 Flat plate planar cross flow design and materials used in the Danish SOFC Programme.

c) evaluation of glass stability in air and hydrogen fuel gas at the SOFC working temperature (1000 °C), analysed by weight loss measurements, and d) analysis of glass compatibility with the SOFC interconnect material with respect to bonding ability and chemical interaction.

2. Experimental

Table I gives, in mole percentage, the batch compositions of the four studied compositions. P_2O_5 is the main glass former but B_2O_3 is added as a fluxing agent and to further enhance the glass forming ability. A is the base material and three compositional variations were performed on the base glass: substitution of MgO with CaO (B), addition of Cr_2O_3 (C) and addition of Cr_2O_3 and CaO (D).

2.1. Glass preparation

The glasses were made from reagent grade $MgHPO_4 \cdot 3H_2O$, $CaHPO_4$, AlP_3O_9, Al_2O_3, H_3BO_3 and Cr_2O_3. The starting materials were weighed and mixed by mortar and pestle followed by ball milling for 1 h. The batches were subsequently melted in alumina crucibles at 1500 °C for 30 min and the melts were homogenized twice by stirring during the dwell time at 1500 °C. After melting, glass fibres were drawn for the stability tests and the remaining glass was cast onto graphite plates. All the manufactured glasses were homogeneous and transparent.

2.2. Thermal analysis and properties

The glass transition point (T_g) and crystallization temperature (T_d) were determined with DTA. The analyses were performed in air on powdered samples ($\sim$ 20 mg passed through a 100 μm sieve). The DTA equipment was a Seiko DSC320 and the heating rate used was 10 °C min^{-1}.

TABLE I Batch compositions of the glasses in mole %

	A	B	C	D
P_2O_5	50.5	50.5	46.5	42.5
B_2O_3	11.3	11.3	11.3	11.3
Al_2O_5	12.6	12.6	11.6	10.6
MgO	25.6		25.6	25.6
CaO		25.6		5.0
Cr_2O_3			5.0	5.0
$P_2O_5 + B_2O_3$	61.8	61.8	57.8	53.8
$Al_2O_3 + Cr_2O_3$	12.6	12.6	16.6	15.6
MgO + CaO	25.6	25.6	25.6	30.6

The linear thermal expansion coefficient (TEC) and T_g (dilatometric) were determined by dilatometric measurement of annealed samples 20 mm in length. The measurements were performed in air on a Netzsch dilatometer, with a heating rate of 2 °C min^{-1}.

2.3. Stability (weight loss) tests

The glass stability tests under cathodic or anodic conditions were performed by a fibre method, where glass fibres of a known dimension are placed onto an inert substrate. The samples were heat treated for 12 h at 1000 °C in either air (cathodic condition) or a fuel gas mixture consisting of 9% hydrogen and 91% nitrogen (anodic condition). The fuel gas is buffered with water to provide a well-defined oxygen partial pressure (pO_2 for the analysis is $\sim 1 \times 10^{-11}$ Pa). This gas mixture will, in the following text, be referred to as wet fuel gas. The samples were weighed before and after heat treatment and the weight losses per surface area calculated.

2.4. Reaction between glass and LCC

The interconnect material chosen for this study is a calcium doped lanthanum chromite, $La_{0.79}Ca_{0.22}CrO_3$ (excess of Ca on the A-site to improve sinterability), referred to as LCC in the following text. The LCC material was synthesized using a glycine nitrate process [9]. Plates were made by uniaxial pressing of powder calcined at 1000 °C for 8 h and sintered at 1450 °C for 2 h. After sintering, the plates were machined to obtain flat, even, surfaces and samples of approximately $10 \times 15 \times 5$ mm were cut. Glass samples of approximately $7 \times 7 \times 10$ mm were cut and ground on one side to ensure good contact with the LCC substrate.

The glass samples were placed on top of the LCC plates, so that they rested in light contact, and heat treated for 24 h in air at 1000, 1100 or 1200 °C to simulate an actual SOFC stack sealing procedure.

After the heat treatments, polished cross-sections of samples were made and the glass to LCC interfaces were examined using scanning electron microscopy (SEM) (JEOL 840). The interfaces are all represented as back scattered electron images (BEI) to enhance the differences in the elemental distribution (except for Fig. 5a where a secondary electron image (SEI) is shown to provide an impression of the LCC

microstructure). The qualitative chemical analyses were performed with energy dispersive spectroscopy (EDS). It should be noted that boron could not be detected with the available EDS system and boron is consequently not considered in great detail in the following discussion.

XRD was performed on the bulk of the glass samples heat treated at 1200 °C to determine the crystalline phases present (Stoe Θ/Θ diffractometer).

3. Results

3.1. Differential thermal analysis (DTA)

The DTA traces are shown in Fig. 2. The T_g and T_d values discussed in the following text refer to extrapolated onset values as indicated in Fig. 2. For sample A, a weak T_g seems to occur around 595 °C (just barely visible on the original trace) but no crystallization peak (T_d) can be observed. Sample B, where MgO has been substituted with CaO, shows a T_g at 602 °C and the sample starts to crystallize at 781 °C. The two chromium containing samples, C and D, show T_g values at 654 and 637 °C, respectively. Sample C has a weak crystallization peak initiating at 796 °C and a strong crystallization peak initiating at 883 °C. Sample D also shows two crystallization peaks: T_{d_1} at 772 °C and T_{d_2} at 873 °C. These values are listed in Table II.

3.2. Dilatometry measurements

The measured expansion curves for the four glasses are shown in Fig. 3 together with curves for LCC and the electrolyte material, 8 mol % yttria stabilized zirconia (8YSZ). The small hump seen on the LCC curve around 275 °C is caused by an orthorhombic or rhombohedral phase transformation [10]. From Fig. 3 it can be seen that the effect of a 5 mole % Cr_2O_3 addition (C) is a slight decrease in the expansion behaviour compared to the base composition (A). The decrease seen in the expansion for sample C is counterbalanced for sample D, where the addition of a small amount of CaO increases the expansion to the same level as the base composition. However, for sample B, where all the MgO has been substituted with CaO, the linear thermal expansion is enhanced significantly in comparison with the other glass compositions and the expansion curve is now close to the LCC curve, but still below the YSZ curve. In Table II the thermal expansion coefficients (TEC) are given for comparison in the temperature range 25–500 °C.

The glass transition temperatures from dilatometry (extrapolated onset, see Fig. 3) for the glasses are also listed in Table II. The T_g for sample A was found to be 603 °C and substitution of Mg with Ca did not change T_g significantly. However, addition of 5 mole % Cr_2O_3 increases T_g by $\sim$ 15 °C as seen for samples C and D. In the latter case, the extra 5 mole % CaO addition does not significantly change T_g.

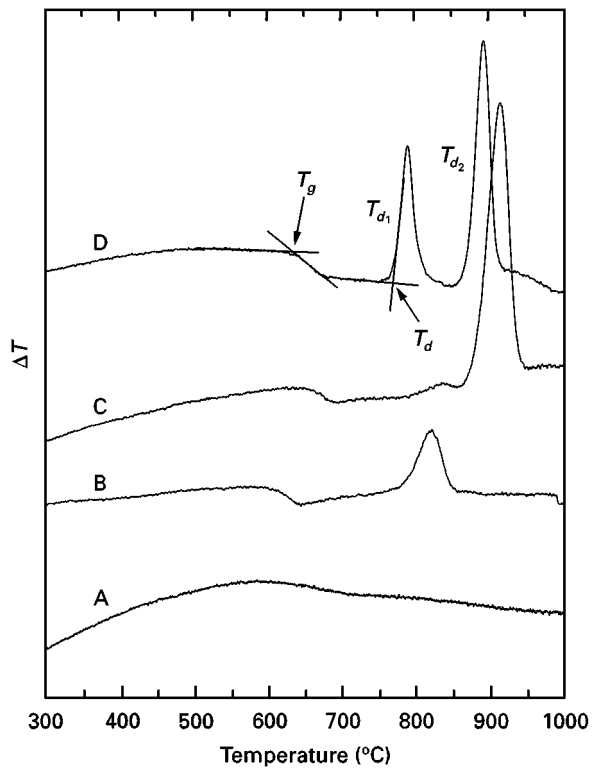

Figure 2 DTA analyses for samples A–D. The determination of onset for T_g and T_d are indicated.

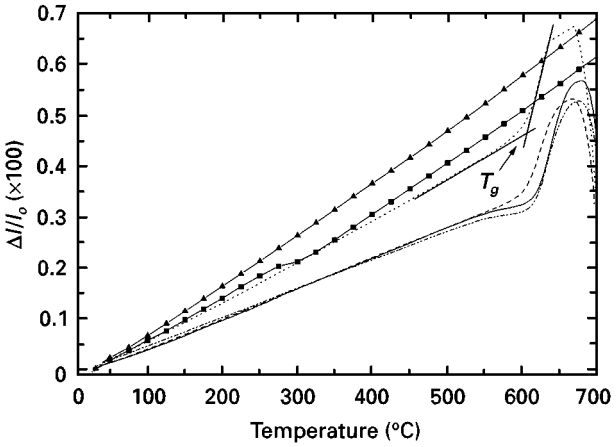

Figure 3 Linear thermal expansion of samples (– –) A, (--) B, (–·–) C, (—) D, $La_{0.8}Ca_{0.22}CrO_3$ (■) and 8 mol % yttria stabilized zirconia (▲): $100 \times \Delta l/l_o$ plotted on Y axis: Δl change in length, l_o original length. The determination of T_g is indicated.

TABLE II Glass transition temperature, T_g (°C) and crystallization temperatures, T_d, (°C) determined by DTA analysis. TEC values given in the temperature range from 25 to 500 °C. The curves are shown in Figs 2 and 3, respectively

	A	B	C	D	LCC	YSZ
DTA: temperature (°C)						
T_g	(595)	602	654	637		
T_{d_1} – extr. onset		781	796	772		
T_{d_1} – peak		824	840	791		
T_{d_2} – extr. onset			883	873		
T_{d_2} – peak			918	894		
$(T_d - T_g)/T_g$		0.25	0.20	0.17		
Dilatometry						
TEC × 10^{-7} K^{-1}	59	79	57	59	85	99
25–500 °C T_g	603	605	618	620		

The T_g values for samples A and B are in agreement with the values measured by DTA, whereas the values for samples C and D differ significantly. The reason for the difference may be related to the relaxation behaviour seen in samples C and D prior to the onset of T_g (Fig. 3).

3.3. Glass forming tendency

The relative glass forming tendency has been evaluated in a number of ways in the literature. One example is the ratio of $(T_d - T_g)/T_g$ (T_g in K) [11], where the relative glass forming tendency decreases as the ratio approaches zero. The values of $(T_d - T_g)/T_g$ listed in Table II are calculated using peak temperatures and they have only been calculated for samples B–D since sample A did not show any crystallization peak on the DTA trace. Based on these considerations, the glass forming tendency appears to be strongest for the base composition (A) followed by sample B with sample C and D as the least stable glass compositions.

3.4. Stability weight loss tests

The volatility losses during heat treatment at 1000 °C, which is considered to be mainly P_2O_5, are shown in Table III. It is quite clear that sample A has the lowest stability and that substitution of Mg with Ca significantly increases the stability in both atmospheres. Addition of Cr_2O_3 also suggests a general decrease in the volatile loss in comparison with sample A, with the least volatility for sample D.

3.5. Reactions between glasses and LCC

Before the heat treated samples were prepared for SEM analysis the bonding to the LCC plates was evaluated and the results are listed in Table IV. The glasses can be divided into three groups in that glass A only bonds to LCC at 1200 °C, glass C bonds at both 1100 and 1200 °C and finally glasses B and D that show bonding even at 1000 °C.

Figs 4 and 5 show glass-LCC interfaces for the heat treated samples. The samples that did not attach to the LCC after heat treatment were replaced as close as possible at the same position as during heat treatment, before embedding in resin. Since exact positioning proved difficult, there were small topographical

TABLE III Weight loss after heat treatment at 1000 °C in air for 12 h in either wet fuel gas or air. The values are given in mg cm^{-2} h^{-1}

Atmosphere	A	B	C	D
Wet fuel gas	1.4	0.2	0.6	0.2
Air	0.6	0.2	0.2	0.2

TABLE IV Indicates whether the glass bonded (+) to the LCC plate or not (−) after the heat treatment at 1000, 1100 or 1200 °C

Temperature (°C)	A	B	C	D
1000	−	+	−	+
1100	−	+	+	+
1200	+	+	+	+

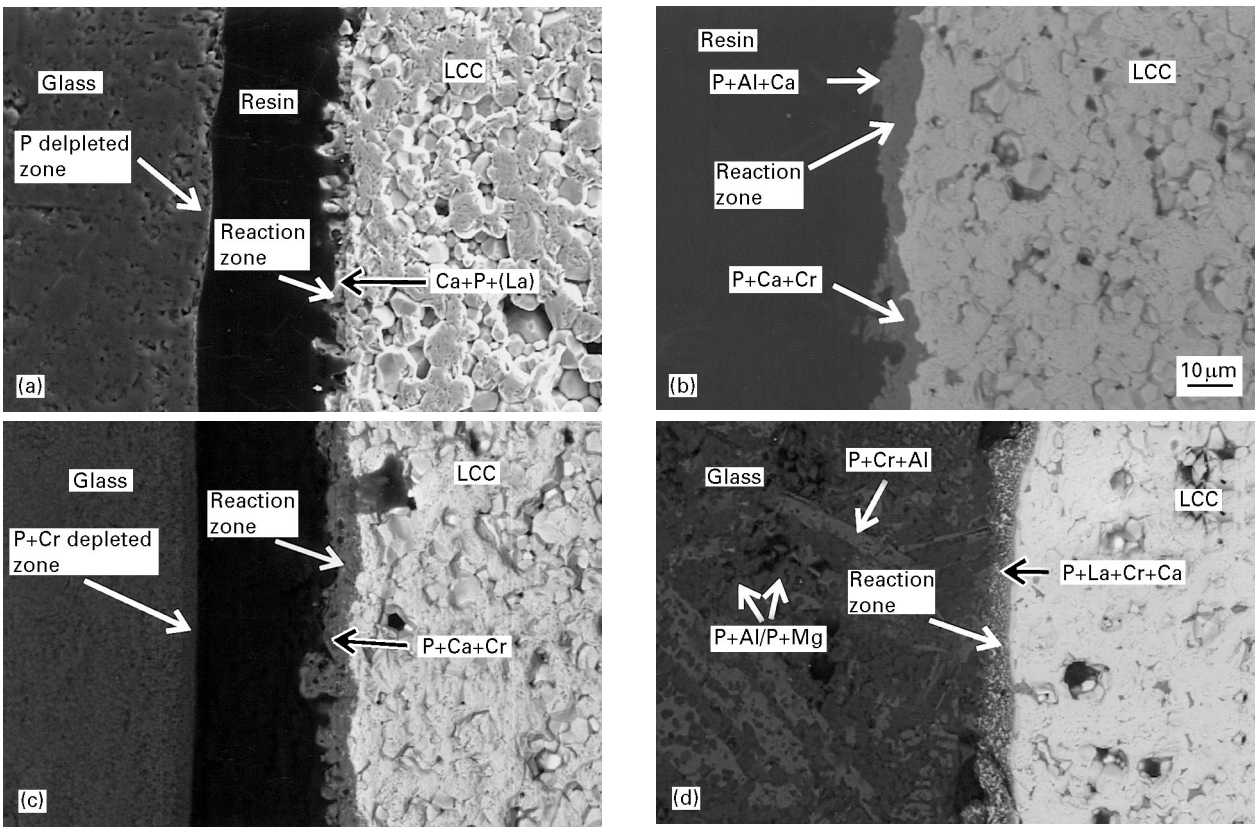

Figure 4 SEM micrographs showing glass/LCC interfaces heat treated in air at 1000 °C for 24 h. Elemental analysis performed with EDS. Sample A represented as secondary electron image (SEI) and the remaining images are backscattered electron images (BEI). (a) glass A, (b) glass B, (c) glass C and (d) glass D.

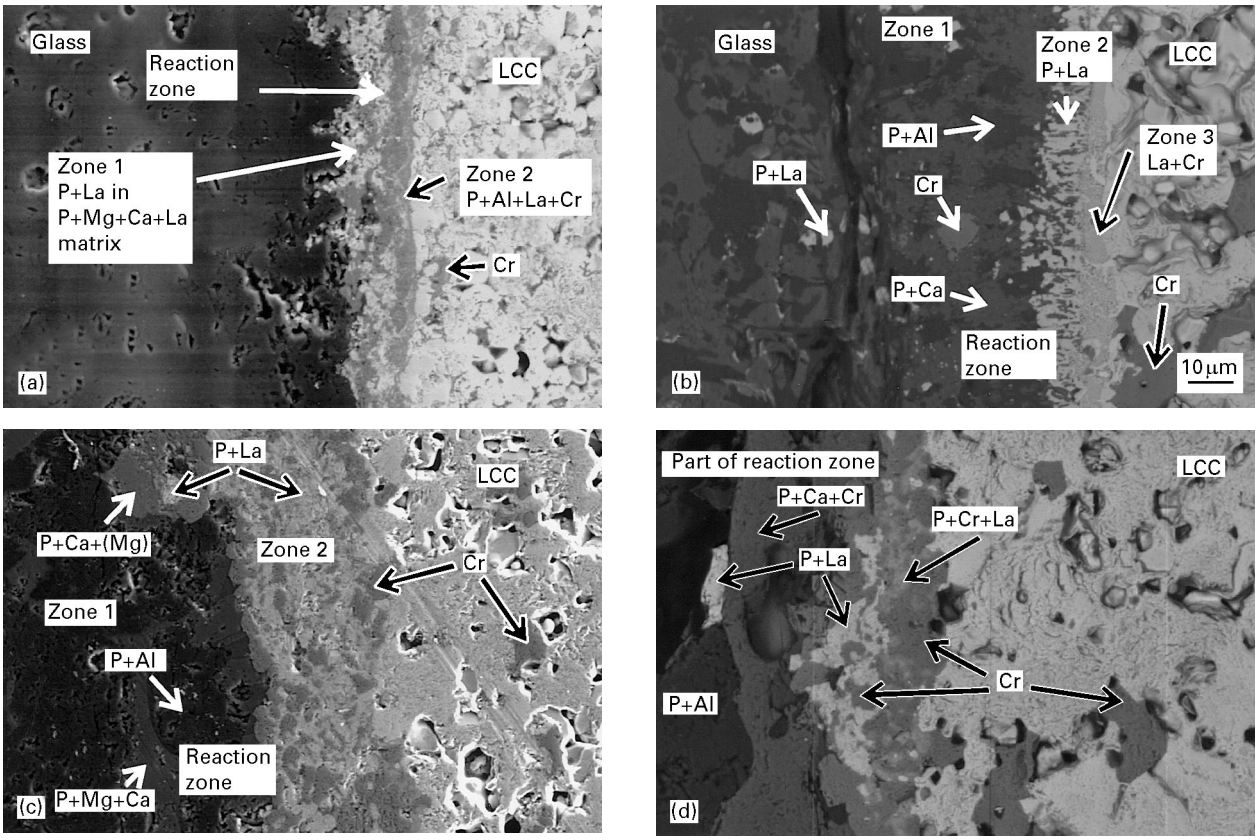

Figure 5 SEM micrographs showing glass/LCC interfaces heat treated in air at 1200 °C for 24 h. Elemental analysis performed with EDS. All images are BEI. (a) glass A, (b) glass B, (c) glass C and (d) glass D.

differences between the glass and the opposed LCC surfaces in the following figures.

Fig. 4a to d show the glass-LCC interfaces for the samples heat treated at 1000 °C. The interface from sample A (Fig. 4a) reveals a 5–10 μm wide reaction zone consisting of grains extending from the LCC surface. The reaction products on the LCC surface consist of Ca and P with traces of La. The outer part of the glass surface is depleted in P and the surface is smooth, thus indicating that no bonding to the LCC has taken place.

The reaction zone for sample B (Fig. 4b) is more coherent. That part of the zone nearest the LCC consists of P, Ca and Cr, and the outer part of the zone nearest the glass has a high concentration of P and Al with some Ca. The fractured appearance of the LCC/glass interface indicates bonding between the components and the separation between glass and LCC has probably occurred as a result of differential contraction in the plane of the interface during cooling (glass side of the reaction zone is not present on Fig. 4b).

Sample C did not bond to the LCC, and the interface (Fig. 4c) is similar to that for sample A both with respect to morphology of the reaction product and the smooth glass surface. The reaction product consists of P and Ca with some Cr. The outer 3 μm on the glass surface is depleted in P and Cr.

In contrast to the other samples, a significant concentration of La is found in the reaction product of sample D (Fig. 4d). Other elements in the reaction zone are P, Cr and Ca. This sample shows a good bonding between the glass and LCC as well as an extensive crystallization in the glass. The crystalline phases in a 100 μm band against the interface comprises up to 50 μm long narrow CrAl-phosphate grains and smaller Mg- and Al-phosphate grains. This area has a low concentration of Ca.

Common for the samples heat treated at 1200 °C is a more significant reaction between glass and LCC together with a more pronounced crystallization in the glass bulk. However, despite the strong interface reaction, glass components were never found to diffuse into the bulk of the LCC.

As mentioned previously, all the glasses bonded to the LCC after heat treatment at 1200 °C. Another common feature for the 1200 °C samples is the presence of Cr_2O_3 grains/layers inside or close to the interface reaction zone and showing an increase in concentration as the degree of reaction increases.

The interfaces for samples A–D are shown in Fig. 5a to d, respectively. Sample A, Fig. 5a, shows a $\sim$ 20 μm broad reaction zone that can be divided roughly into 2 sub-zones with varying compositions. Zone 1, starting from the un-reacted glass, has a P + Mg + Ca + La bulk phase with small light grains of P + La. Zone 2, a $\sim$ 5 μm band next to the unreacted LCC, consists of P + Al + La + Cr. A few Cr_2O_3 grains are found in the LCC close to the reaction zone. Ca diffusion is found up to 1 mm inside the glass.

The interface reaction region for sample B (Fig. 5b) extending from the LCC to the crack parallel to the interface, is 60 μm wide. The reaction region is divided

into three zones, zone 1 going from the fracture crack towards the LCC consists of four phases: P + Al, P + Ca, Cr and P + La. In Zone 2, a 10 μm band shows a strong interdiffusion, this area has a high concentration of P + La. Zone 3 is a layer with La and Cr as the only elements. Significant diffusion of La is found up to 250 μm inside the glass where La appears together with P. Cr_2O_3 grains are again found in the LCC bulk close to the reaction zone.

Sample C (Fig. 5c) has a 100–120 μm wide interface reaction region divided into two zones. Zone 1 closest to the glass has a number of different phases: P + Al, P + Mg + Ca and P + Ca + (Mg) with small inclusions of P + La (brackets indicate that only a trace of the element is present). Zone 2 between zone 1 and the un-reacted LCC shows Cr and P + La. As for the previous samples Cr_2O_3 grains are found in the LCC.

The interface region for sample D is quite complex compared to the other samples, and reveals a reaction zone with spherical pores up to 300 μm diameter with reaction products on both sides (image also not shown here). The area between the porous zone and the bulk glass reveals a variety of phases: P + Al, P + Mg, P + La + (Cr), P + Ca + Cr, P + Cr + Al and P + Ca + La + Cr (image also not shown here). The inner part of the reaction zones closest to the LCC (seen on Fig. 5d) shows four areas starting with grey Cr_2O_3 layer in the contact to the LCC (area 1). Moving away from the LCC, area two has a Cr_2O_3 phase together with a P + Cr + La phase. Area 3 has the same Cr_2O_3 phase but now the second phase consists of P + La and, finally, area 4 that is followed by the porous area has only one phase containing P + Ca + Cr.

3.6. Glass bulk

No images are shown here from the 1000 °C bulk samples. Samples B–D showed bulk crystallization whereas no visible signs of crystallization were observed in the bulk of sample A. EDS analysis results are shown in Table V. At 1200 °C, crystallization had taken place in all the samples. Images from the bulk glasses are shown in Fig. 6a to d and the phases determined by EDS are listed in Table V. XRD was

TABLE V Phases determined by EDS and XRD in the bulk of the samples

Sample	EDS 1000 °C	EDS 1200 °C	XRD 1200 °C
A	No crystallization	P + Al in a P + Al + Mg matrix	$AlPO_4$, amorphous phase
B	P + Al in a P + Al + Ca matrix	P + Ca and P + Al in a P + Ca + Al matrix	$Ca_2P_2O_7$, $AlPO_4$ major unknown peaks, amorphous phase
C	Not analysed due to small grain size	P + Al, P + Mg, P + Cr + Al and P + Mg + Al + Cr matrix	$AlPO_4$, $Mg_2P_2O_7$, unknown phase(s), amorphous phase
D	P + Al in a P + Mg + Ca + Cr matrix	P + Al, P + Mg, P + Cr + Al and P + Ca + Mg + Cr matrix	$AlPO_4$, $Mg_2P_2O_7$, unknown phase(s), amorphous phase

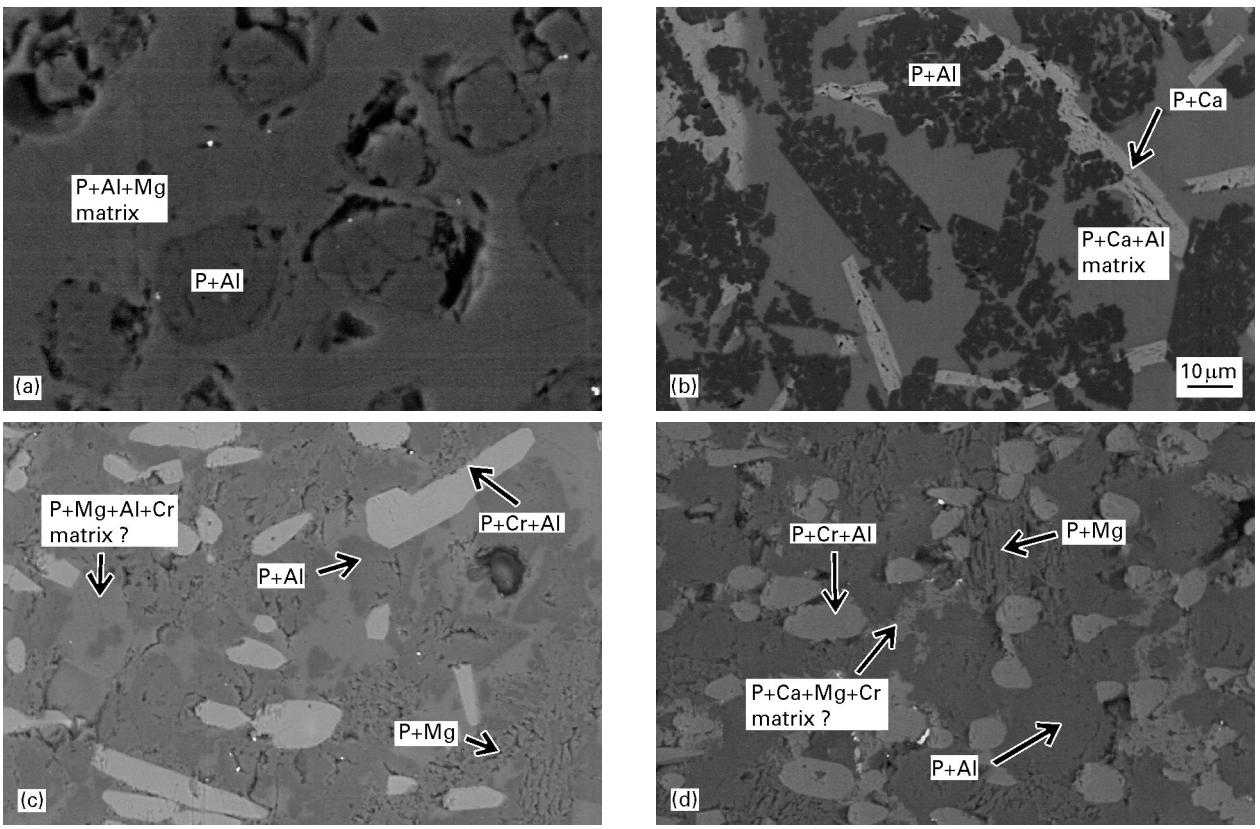

Figure 6 SEM micrographs from bulk glasses. Samples heat treated in air at 1200 °C for 24 h. Elemental analysis performed with EDS. All images are BEI. (a) glass A, (b) glass B, (c) glass C and (d) glass D.

performed on bulk glass samples heat treated at 1200 °C (Table V). All the samples show the presence of an amorphous phase and $AlPO_4$. Sample B has additionally $Ca_2P_2O_7$ together with a major unknown phase, whereas samples C and D both have $Mg_2P_2O_7$ together with a number of unknown peaks.

There is a good correspondence between the compositions of the phases found by XRD and EDS for the Mg- and Al-phosphate phases, but sample B showed two major peaks that could not be matched by the JCPDS database. The diffraction patterns for samples C and D are similar and the undetermined peaks probably in these cases represent Cr-phosphate with Al in solid solution as indicated by the EDS analysis.

For all the samples, an amorphous peak was observed and the relative intensity was highest for sample A. The elemental compositions of the amorphous phases are probably as given by the EDS analysis for the matrix composition. It is assumed that boron also is to be found in the matrix.

4. Discussion

4.1. Glass stability

Kishioka *et al.* [12] have studied glass formation in the ternary MgO and CaO-Al_2O_3-P_2O_5 systems. The data of Kishioka, reproduced in Fig. 7, show that CaO has a smaller glass forming region than MgO.

To compare the glass forming tendency for the compositions studied here with the glass forming regions in Fig. 7 the batch compositions are re-calculated to give a ternary system in the following way: glass former = $P_2O_5 + B_2O_3$, MO = MgO + CaO and $M_2O_3 = Al_2O_3 + Cr_2O_3$. The ternary systems thus calculated (Table I) plotted in Fig. 7 show that all 4 compositions lie within the relevant glass forming regions and that their positions agree well with the relative glass forming tendencies as indicated by T_g and crystallization temperature (T_d) values (Table II).

4.2. Weight losses

The decrease in weight loss of volatiles under SOFC atmospheric conditions for samples B–D relative to sample A seems to be related to the glass forming tendency, or in other words, to the stability of the glass structure. P_2O_5 volatilization from the glass surface will lower the P_2O_5 concentration in the residual glass, and this will cause the composition to move towards the border of, or even outside of, the glass forming region. A consequence is that crystallization will occur more readily. Since the crystalline phases are expected to have a lower P_2O_5 vapour pressure than the initial glass, the loss of P_2O_5 from the surface will consequently decrease as crystallization proceeds.

From Fig. 7 it is evident that glass A has to lose more P_2O_5 relatively to glass B to move outside the glass forming region in question. A similar argument may be applied when comparing glasses A, C and D, where the weight loss decreases as the glass forming tendency decreases and the composition moves towards the boundary of the glass forming region. However, since there is an overall decrease in the P_2O_5 concentration in going from A to C to D, this will, of course, limit the total possible loss of P_2O_5 and perhaps also the loss rate.

4.3. Reaction mechanisms between glasses and LCC

The sintering mechanism of the LCC material is a Ca excess liquid phase assisted by a $Ca_m(CrO_4)_n$ ($n \leqslant m$) liquid phase [13] where the formation of the liquid

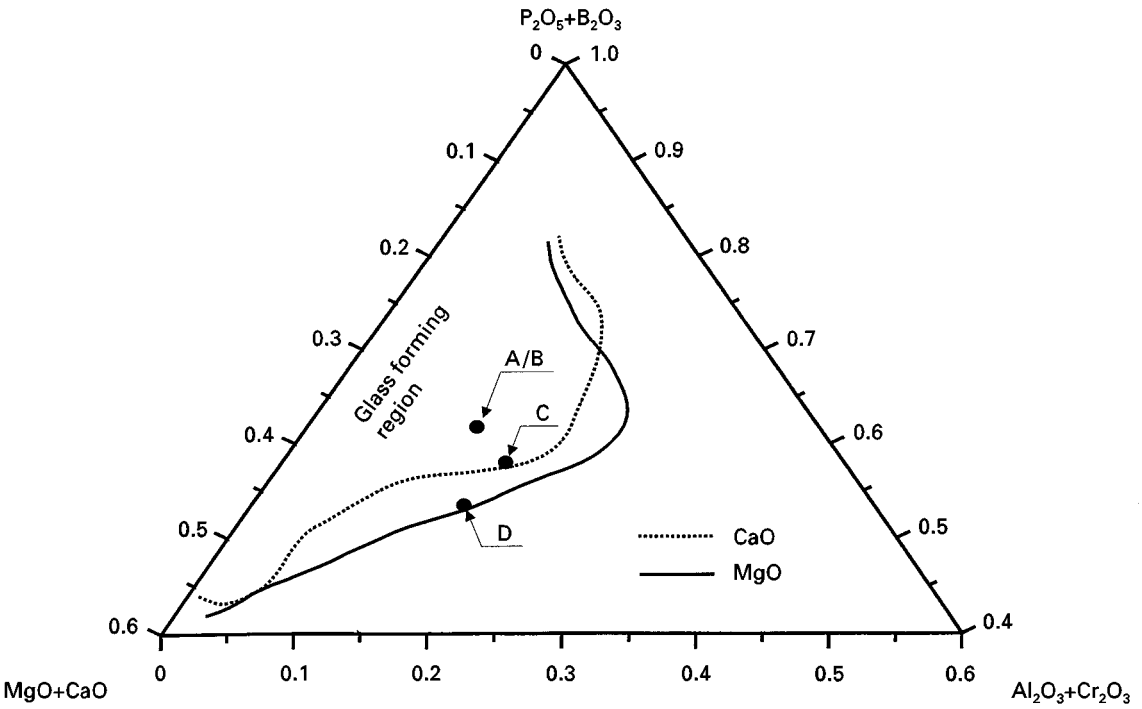

Figure 7 Glass forming regions for the ternary MgO/CaO-Al_2O_3-P_2O_5 systems determined by Kishioka *et al.* [12]. Samples A–D are plotted as glass former-MO-M_2O_3 ternary systems where glass former = $P_2O_5 + B_2O_3$ MO = MgO + CaO and $M_2O_3 = Al_2O_3 + Cr_2O_3$.

phase is initiated above 1022 °C [14]. After sintering of the LCC, part of this liquid phase will remain in the grain boundaries. XRD analysis of the LCC material revealed the secondary phase to be $CaCrO_4$.

The difference in reaction type and interface appearance between samples with or without CaO (glasses B and D and glasses A and C, respectively) at 1000 °C may, to a large extent, be ascribed to the generally lower melting points of CaO containing compositions compared to MgO compositions in these systems. This is evident when comparing the MgO/CaO–Al_2O_3–P_2O_5 systems [15–17] as illustrated in Fig. 8 by the Mg- and Ca-Al-metaphosphate binaries that represent the boundary curves in the high P_2O_5 region of the relevant phase fields ($Mg/Ca(PO_3)_2$–$Al(PO_3)_2$–$AlPO_4$). The temperature difference in the binary eutectic points is 130 °C with a eutectic temperature for the CaO containing system at 925 °C. A part of the phase distribution for glass B will be a thermodynamically stable liquid phase at 1000 °C and a higher reactivity of the CaO glasses is to be expected.

The relatively strong bonding with LCC for glass D, that has a low CaO concentration, may additionally be influenced by the relative higher crystallization tendency of this glass. Assuming that the crystalline phases are pyro- and orthophosphates, the concentration of P_2O_5 in the glass will be significantly higher than in the crystals. Since the rate of vapour loss is relatively limited in the interface area the concentration of P_2O_5 will continuously increase in the residual glass as crystallization proceeds, thus causing a decrease in liquidus temperature of the residual glass and thereby an enhanced reactivity. The suggested reaction mechanism for samples B and D with a reactive liquid from the glass is shown in Equation 1.

$$\text{glass(1)} + CaCrO_4(s) + (La, Ca)CrO_3(s) \rightarrow \text{Ca/Cr/La-phosphates (l, s)} \quad (1)$$

The reaction mechanism at 1000 °C for the more viscous MgO containing samples which do not bond (glasses A and C) is thought to be by vapour phase transport of P_2O_5 to the LCC surface where it reacts as indicated in Equation 2.

$$P_2O_5(g) + CaCrO_4(s) + (La, Ca)CrO_3(s) \rightarrow \text{Ca/Cr/La-phosphates(s)} \quad (2)$$

At 1200 °C the reactions are more severe, in general, and the LCC material plays a more active role since the LCC will have a liquid phase in the grain boundaries that readily reacts with the glass.

The degree of reaction at 1200 °C increases on going from glass A to glass D. The reaction products show a variety of different elemental distributions. Diffusion of Ca up to 1000 μm from the interface is seen for glass A and La has diffused more than 250 μm inside glass B, Diffusion of Cr is also seen but to a much smaller extent. Instead, the presence of Cr_2O_3 in and close to the reaction zone is a feature common to all the samples and seen with higher concentrations occurring for the greater degrees of reaction at the interface.

The relatively high concentration of the Cr_2O_3 phase in the interface regions of the 1200 °C samples indicates that Cr_2O_3 precipitates from the melt formed at the interface as suggested schematically by Equation 3. Sol indicates components that are dissolved in the liquid phase in the interface region.

$$\text{glass(l)} + CaCrO_4(l) + (La, Ca)CrO_3(s) \rightarrow La_2O_3/CaO/Cr_2O_3(sol) + \text{glass(l)} + Cr_2O_3(s) + O_2(g) \quad (3)$$

A similar type of reaction has been observed for a SiO_2 glass by Horita *et al.* [6]. It is interesting to note that a reduction of chromium takes place during the reaction and this formation of oxygen may be responsible for the development of porosity.

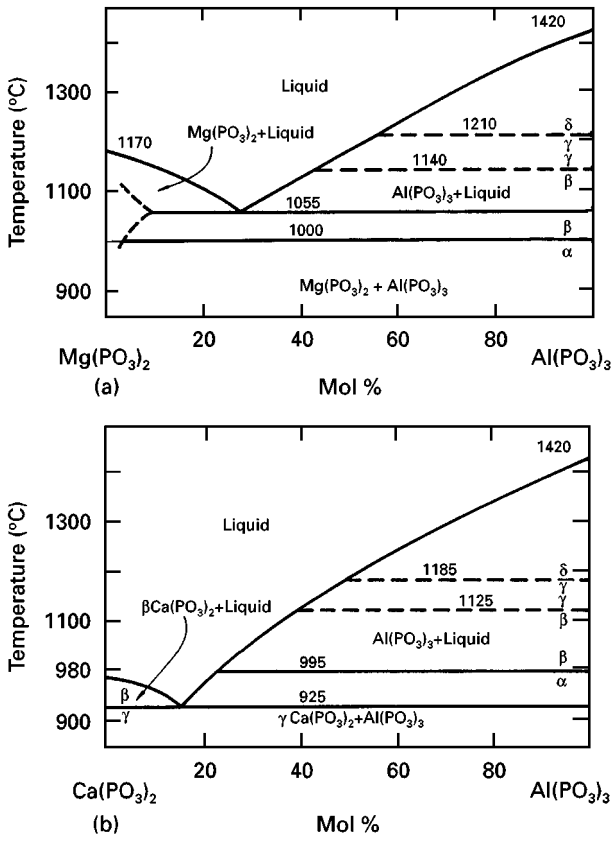

Figure 8 $Mg/Ca(PO_3)_2$-$Al(PO_3)_3$ binary systems taken from [17].

5. Conclusion

The thermal properties, relative glass forming tendency and weight losses in SOFC relevant atmospheres as well as interaction with LCC interconnect material have been investigated for a number of phosphate based glass compositions. The four compositions studied were a MgO–Al_2O_3–B_2O_3–P_2O_5 base composition (A) and three systematic compositional variations: MgO substituted with CaO (composition B), addition of Cr_2O_3 (composition C) and addition of CaO and Cr_2O_3 (composition D).

Substitution of MgO with CaO was found to increase the TEC from $59 \times 10^{-7}\,K^{-1}$ to $79 \times 10^{-7}\,K^{-1}$ (25 to 500 °C) which, in the latter case, only differs by 8% from the value for LCC. Addition of Cr_2O_3 had a small negative effect on the TEC. The thermal expansion properties of the (fully) crystallized materials

were not examined but will be relevant for a long term application that includes thermal cycling.

The glass forming tendencies, as indicated by T_g and crystallization temperature (T_d), were in accordance with predictions from ternary phase diagrams and published glass forming boundaries. It was also shown that the glass stability with respect to volatile losses is related to the glass forming tendency. A decrease in glass forming tendency decreases the volatile loss.

The bonding abilities of the glasses were found to be closely related to the CaO content and the relative glass forming tendency. Both glasses containing CaO bonded to the LCC even at 1000°C, which is explained by the relatively lower melting points in the CaO system that provides a thermodynamically stable liquid at 1000 °C. In the case of MgO the reaction is caused by vapour phase transport of P_2O_5 to the LCC surface where it reacts. At 1200 °C a more severe reaction takes place due to liquid–liquid interaction.

The presence of Cr(VI) in the form of $CaCrO_4$ may cause pore formation inside the seal if severe reactions take place at the interface. This may not only create leakages in the seal but will also reduce the mechanical strength.

Based on the experimental results it can be concluded that glass B is the most suitable for SOFC application because bonding can be achieved at 1000 °C without severe reactions. Moreover, glass B has a relatively high TEC as well as the lowest tendency to volatile loss. However, even for sample B the volatile loss is significant and the influence of volatile phosphorus species in the SOFC environment will require further investigation.

Acknowledgements

This work was supported by the Danish Energy Agency and the Danish electrical utility ELSAM under the DK-SOFC Programme. PFJ James thanks EPSRC (GR/J69073) for support.

References

1. P. H. LARSEN, C. BAGGER, M. MOGENSEN and J. G. LARSEN, in Proceedings of the Fourth International Symposium on Solid Oxide Fuel Cells (SOFC-IV), 1995, vol. 95-1, edited by M. Dokiya, O. Yamamoto, H. Tagawa and S. C. Singhal, (The Electrochemical Society Inc., Pennington, NJ) 69.
2. C. BAGGER, P. V. HENDRIKSEN and M. MOGENSEN, in Proceedings of the First European Solid Oxide Fuel Cell Forum, 1994, edited by U. Bossel. Lucerne, Switzerland, (1994) 691.
3. P. H. LARSEN, S. PRIMDAHL and M. MOGENSEN, in Proceedings of the Seventeenth Risø International Symposium on High Temperature Electrochemistry: Ceramics and Metals, Risø National Laboratory, Denmark, 1996, edited by F. W. Poulsen, N. Bonanos, S. Linderoth, M. Mogensen, and B. Zachau-Christiansen, p. 331.
4. T. YAMAMOTO, H. ITOH, M. MORI, N. MORI and T. ABE, in Proceedings of the Fourth International Symposium on Solid Oxide Fuel Cells (SOFC-IV), 1995, vol 95-1, edited by M. Dokiya, O. Yamamoto, H. Tagawa and S. C. Singhal (The Electrochemical Society Inc., Pennington, NJ) 245.
5. H. YOKOKAWA, T. HORITA, N. SAKAI, T. KAWADA and M. DOKYA, in Proceedings of the Fourteenth Risø International Symposium on High Temperature Electrochemical Behaviour of Fast Ion and Mixed Conductors, Risø National Laboratory, Denmark, 1993, edited by F. W. Poulsen, J. J. Bentzen, T. Jacobsen, E. Skou and M. J. L. Østergård, p. 473.
6. T. HORITA, J. CHOI, Y. LEE, N. SAKAI, T. KAWADA, H. YOKOKAWA and M. DOKIYA, *J. Am. Ceram. Soc.* **78** (1995) 1729.
7. T. W. KEUPER and I. D. BLOOM, in Proceedings of the Second International Conference on Heat-Resistant Materials, 1995, Gatlinburg, Tennessee, USA. 11–14 September, edited by K. Natesan, P. Ganesan and G. Y. Lei, (ASM International, Materials Park, Ohio) 545.
8. K. L. LEY, M. KRUMPELT, R. KUMAR, J. H. MEISER and I. J. BLOOM, *J. Mater. Res.* **11** (1996) 1489.
9. L. CHICK, J. BATES, L. PEDERSON and H. KISSINGER, in Proceedings of the First International Symposium on Solid Oxide Fuel Cells (SOFC-I), 1989, vol 89–11, edited by S. C. Singhal, (The Electrochemical Society Inc., Pennington, NJ) 170.
10. N. SAKAI, T. KAWADA, H. YOKOKAWA, M. DOKIYA and T. IWATA, *Solid State Ion.* **40/41** (1990) 394.
11. M. OUCHETTO, B. ELOUADI and S. PARKE, *Phys. Chem. Glasses* **32** (1991) 22.
12. A. KISHIOKA, M. HAYASHI and M. KINOSHITA, *Bull. Chem. Soc. Jpn.* **49** (1976) 3032.
13. N. SAKAI, T. KAWADA, H. YOKOKAWA, M. DOKIYA and I. J. KOJIMA, *J. Am. Ceram. Soc.* **76** (1993) 609.
14. J. D. CARTER, M. M. NASRALLAH and H. U. ANDERSON, *J. Mater. Sci.* **31** (1996) 157.
15. F. J. GONZALEZ and J. W. HALLORAN, *J. Am. Ceram. Soc.* **63** (1980) 599.
16. P. E. STONE, E. P. EGAN and J. R. LEHR, *ibid.* **39** (1956) 96.
17. M. I. KUZMENKOV, S. V. PLYSHEVSKI, I. PLYSHEVSKI and V. V. PECHKOVSKII, *Inorg. Mater.* **10** (1974) 1581.

Received 18 November 1997
and accepted 13 February 1998